

TCDA: ROBUST 2D-DOA ESTIMATION FOR DEFECTIVE L-SHAPED ARRAYS

Wenlong Wang^{1†}, Tianyang Zhang^{2†}, Tailun Dong³ and Lei Zhang^{1*}

¹ School of Integrated Circuits, Tsinghua University, China

² School of Information and Communication Engineering,

University of Electronic Science and Technology of China, China

³ School of Communications and Information Engineering & School of Artificial Intelligence,
Xi'an University of Posts and Telecommunications, China

ABSTRACT

While tensor-based methods excel at Direction-of-Arrival (DOA) estimation, their performance degrades severely with faulty or sparse arrays that violate the required manifold structure. To address this challenge, we propose Tensor Completion for Defective Arrays (TCDA), a robust algorithm that reformulates the physical imperfection problem as a data recovery task within a virtual tensor space. We present a detailed derivation for constructing an incomplete third-order Parallel Factor Analysis (PARAFAC) tensor from the faulty array signals via subarray partitioning, cross-correlation, and dimensional reshaping. Leveraging the tensor's inherent low-rank structure, an Alternating Least Squares (ALS)-based algorithm directly recovers the factor matrices embedding the DOA parameters from the incomplete observations. This approach provides a software-defined 'self-healing' capability, demonstrating exceptional robustness against random element failures without requiring additional processing steps for DOA estimation.

Index Terms— Direction of Arrival (DOA) Estimation, L-shaped Array, Tensor Decomposition, Parallel Factor Analysis (PARAFAC), Tensor Completion, Faulty Array, Alternating Least Squares

1. INTRODUCTION

DOA estimation is a fundamental task in radar, sonar, and wireless communications [1, 2]. L-shaped arrays are common for 2D DOA estimation [3], where tensor-based methods like PARAFAC offer automatic parameter pairing and increased degrees of freedom (DOF) [4, 5]. However, these methods rely on a precise array manifold and suffer catastrophic performance degradation from sensor failures that corrupt the array's Vandermonde structure. Conventional solutions

like hardware maintenance are costly, while calibration algorithms are often complex and suboptimal.

This paper introduces TCDA, a novel software framework that treats a physically faulty array as an incomplete sampling of an ideal data structure [6]. Unlike Compressed Sensing (CS) strategies that flatten array data into vectors, potentially severing inherent multidimensional dependencies [7], TCDA operates directly on the high-order tensor structure. This preservation of spatiotemporal correlations is conceptually advantageous for handling array defects, although a detailed comparison with vector-based sparse recovery is beyond the scope of this initial work. While related to virtual array concepts [8, 9], our key distinction is a process starting from raw signals. We construct an incomplete third-order tensor via subarray partitioning, cross-correlation, and reshaping. The tensor's ideal low-rank PARAFAC structure ensures identifiability [10], reformulating the DOA problem as a weighted PARAFAC decomposition with missing data [11]. An ALS-based algorithm then "interpolates" the missing data to directly recover the factor matrices containing the paired 2D DOA information [12].

This data "healing" process directly yields the factor matrices for DOA estimation, enhancing efficiency and accuracy [13]. Our contributions are: a) we model the incomplete target tensor from faulty array signals; b) we formalize DOA estimation for faulty arrays as a weighted PARAFAC task; and c) we derive the ALS-based TCDA algorithm, demonstrating its robust, high-accuracy performance on arrays with substantial faults [14].

2. SIGNAL MODEL AND PROBLEM FORMULATION

2.1. Ideal Array Signal and Data Tensors

Consider an L-shaped array consisting of two orthogonal M -element Uniform Linear Arrays (ULAs) on the x - and z -axes. K uncorrelated far-field narrowband signals impinge from directions $\{(\phi_k, \theta_k)\}$. We partition the x -ULA into N_x overlapping subarrays of size L_{x1} and the z -ULA into N_z subarrays

[†]These authors contributed equally to this work.

*Corresponding author: Lei Zhang (email: zhang.lei@tsinghua.edu.cn).

This work was supported by the National High Technology Research and Development Program of China under Grant 2021YFB2900403.

of size L_{z1} .

For the x-UULA, the received signal can be structured into a third-order tensor $\mathcal{X} \in \mathbb{C}^{L_{x1} \times N_x \times N}$ (N is the number of snapshots), whose noiseless part can be expressed as:

$$\mathcal{X}_{ideal} = \sum_{k=1}^K \mathbf{a}_{xk}^{(1)} \circ \mathbf{b}_{xk} \circ \mathbf{s}_k, \quad (1)$$

where \circ denotes the outer product and $\mathbf{s}_k \in \mathbb{C}^{N \times 1}$ is the waveform vector of the k -th signal. The factor vectors are constructed based on the term $\Theta_k = e^{j\pi \cos \theta_k}$, where $\mathbf{a}_{xk}^{(1)} = [\Theta_k, \Theta_k^2, \dots, \Theta_k^{L_{x1}}]^T \in \mathbb{C}^{L_{x1} \times 1}$ is the steering vector of the first subarray, and $\mathbf{b}_{xk} = [1, \Theta_k, \dots, \Theta_k^{N_x-1}]^T \in \mathbb{C}^{N_x \times 1}$ contains the phase relationship between subarrays.

Similarly, for the z-UULA, we have the data tensor $\mathcal{Z} \in \mathbb{C}^{L_{z1} \times N_z \times N}$:

$$\mathcal{Z}_{ideal} = \sum_{k=1}^K \mathbf{a}_{zk}^{(1)} \circ \mathbf{b}_{zk} \circ \mathbf{s}_k, \quad (2)$$

where $\mathbf{a}_{zk}^{(1)} = [1, \Phi_k, \dots, \Phi_k^{L_{z1}-1}]^T$, $\mathbf{b}_{zk} = [1, \Phi_k, \dots, \Phi_k^{N_z-1}]^T$, and $\Phi_k = e^{j\pi \cos \phi_k}$.

2.2. Virtual Array Construction and Target Tensor

We compute the cross-correlation between \mathcal{X} and \mathcal{Z} along the snapshot dimension, yielding a fourth-order tensor $\mathcal{R}_{xz} \in \mathbb{C}^{L_{x1} \times N_x \times L_{z1} \times N_z}$:

$$\begin{aligned} \mathcal{R}_{xz} &= \mathbb{E}\{\mathcal{X}(:, :, n) \circ \mathcal{Z}(:, :, n)^*\} \\ &= \sum_{k=1}^K \sigma_k^2 \mathbf{a}_{xk}^{(1)} \circ \mathbf{b}_{xk} \circ \mathbf{a}_{zk}^{(1)*} \circ \mathbf{b}_{zk}^*. \end{aligned} \quad (3)$$

Leveraging the conjugate symmetry property of the ULA manifold, we obtain \mathcal{R}_{xz}^* by reversing the dimensions and conjugating \mathcal{R}_{xz} . We then concatenate these two tensors along a new fifth dimension to form an augmented five-order tensor $\mathcal{R} \in \mathbb{C}^{L_{x1} \times N_x \times L_{z1} \times N_z \times 2}$:

$$\mathcal{R} = \sum_{k=1}^K \sigma_k^2 \mathbf{a}_{xk}^{(1)} \circ \mathbf{b}_{xk} \circ \mathbf{a}_{zk}^{(1)*} \circ \mathbf{b}_{zk}^* \circ \mathbf{u}_k, \quad (4)$$

where $\mathbf{u}_k = [1, \Theta_k^{-M-1} \Phi_k^{M-1}]^T$.

As shown in [15], to isolate the angular parameters for estimation, the tensor \mathcal{R} can be effectively rearranged into another five-order tensor \mathcal{Q} :

$$\mathcal{Q} = \sum_{k=1}^K \mathbf{a}_{xk}^{(0)} \circ \mathbf{c}_k \circ \mathbf{a}_{zk}^{(0)*} \circ \mathbf{e}_k \circ \mathbf{p}'_k, \quad (5)$$

where $\mathbf{p}'_k = \mathbf{p}_k \sigma_k^2$ is the equivalent signal, and the newly introduced factor vectors are defined as $\mathbf{c}_k = [1, \Theta_k]^T$, $\mathbf{e}_k = [1, \Phi_k^{-1}]^T$, $\mathbf{a}_{xk}^{(0)} = [\Theta_k, \dots, \Theta_k^{L_{x1}-1}]^T$, and $\mathbf{a}_{zk}^{(0)*} =$

$[1, \Phi_k^{-1}, \dots, \Phi_k^{-L_{z1}+2}]^T$. The equivalent signal vector \mathbf{p}_k is formed by the Kronecker product of the factor vectors from (4) corresponding to the dimensions that will be merged:

$$\mathbf{p}_k = \mathbf{u}_k \otimes \mathbf{b}_{zk}^* \otimes \mathbf{b}_{xk}. \quad (6)$$

Finally, we employ the generalized tensorization operation to merge the dimensions of the five-order tensor \mathcal{Q} , forming the final third-order target tensor \mathcal{T}_{ideal} :

$$\mathcal{T}_{ideal} \triangleq \mathcal{Q}_{\{1,3\}\{2,4\}\{5\}} = \sum_{k=1}^K \mathbf{g}_k \circ \mathbf{h}_k \circ \mathbf{p}'_k. \quad (7)$$

This operation reshapes the tensor \mathcal{Q} into a third-order tensor, $\mathcal{T}_{ideal} \in \mathbb{C}^{L_{x0} L_{z0} \times 4 \times 2 N_x N_z}$, by merging its dimensions $\{1, 3\}$, $\{2, 4\}$, and $\{5\}$. The resulting tensor has a perfect rank- K PARAFAC structure, with factor vectors defined as the virtual array response $\mathbf{g}_k = \mathbf{a}_{zk}^{(0)*} \otimes \mathbf{a}_{xk}^{(0)}$, the angle information vector $\mathbf{h}_k = \mathbf{e}_k \otimes \mathbf{c}_k = [1, \Theta_k, \Phi_k^{-1}, \Theta_k \Phi_k^{-1}]^T$, and the equivalent signal \mathbf{p}'_k . The structure of the vector \mathbf{h}_k is critical for the subsequent DOA estimation.

2.3. Defective Array Model and Final Problem Formalization

We now introduce array defects, which are modeled using binary mask vectors $\mathbf{m}_x, \mathbf{m}_z \in \{0, 1\}^M$, where '1' denotes a functional element and '0' a failed one. The actually observed signals at the array aperture are:

$$\mathbf{x}_{obs}(t) = \text{diag}(\mathbf{m}_x) \cdot \mathbf{x}_{ideal}(t) + \mathbf{w}_x(t), \quad (8)$$

$$\mathbf{z}_{obs}(t) = \text{diag}(\mathbf{m}_z) \cdot \mathbf{z}_{ideal}(t) + \mathbf{w}_z(t), \quad (9)$$

where $\mathbf{w}_x(t)$ and $\mathbf{w}_z(t)$ denote the additive noise vectors. Crucially, a physical failure at the p -th sensor simultaneously corrupts all subarray entries satisfying the index relationship $l + n - 1 = p$. This mechanism induces a structured missing pattern characterized by the loss of entire fibers, which inherently challenges the incoherence conditions typically required for robust recovery.

To determine the reliability of data without prior knowledge of \mathbf{m}_x and \mathbf{m}_z , we employ a blind detection mechanism. Let \mathcal{E} be the amplitude tensor with entries $[\mathcal{E}]_{ijk} = |[\mathcal{T}_{obs}]_{ijk}|$. The binary mask tensor $\mathcal{W}_{\mathcal{T}}$ is determined via an adaptive thresholding scheme:

$$[\mathcal{W}_{\mathcal{T}}]_{ijk} = \mathbb{I}([\mathcal{E}]_{ijk} > \eta_{th}), \quad (10)$$

where $\mathbb{I}(\cdot)$ is the indicator function which equals 1 if the condition is true and 0 otherwise, and η_{th} is the detection threshold. This threshold is defined based on robust energy statistics as:

$$\eta_{th} = \frac{1}{\gamma} \cdot \text{median}(\text{vec}(\mathcal{E})) + \epsilon, \quad (11)$$

where $\text{vec}(\mathcal{E})$ denotes the vectorized form of the amplitude tensor, γ is a sensitivity scaling factor, and ϵ is a small regularization constant ensuring numerical stability.

This process yields the final mask $\mathcal{W}_{\mathcal{T}} \in \{0, 1\}^{L_x \times L_z \times 4 \times 2N_x N_z}$, where $w_{ijk} = 1$ indicates reliable data. Consequently, our observation model is accurately represented as:

$$\mathcal{T}_{obs} = \mathcal{W}_{\mathcal{T}} \times \mathcal{T}_{ideal} + \mathcal{N}_{\mathcal{T}}, \quad (12)$$

where \mathcal{T}_{obs} is the incomplete tensor computed from the defective array data, \times denotes the Hadamard product, and $\mathcal{N}_{\mathcal{T}}$ is the noise tensor.

The core problem of this paper is formalized as: given the incomplete, noisy third-order tensor \mathcal{T}_{obs} and the estimated mask $\mathcal{W}_{\mathcal{T}}$, directly recover the factor matrices $\mathbf{G}, \mathbf{H}, \mathbf{P}$ of the ideal tensor \mathcal{T}_{ideal} .

3. TCDA FRAMEWORK: WEIGHTED PARAFAC DECOMPOSITION

We leverage the low-rank property of \mathcal{T}_{ideal} to complete the missing data and estimate the factor matrices by solving a weighted PARAFAC decomposition problem.

3.1. Mathematical Formulation

Our goal is to find a rank- R (where R is the estimate of the number of sources, K) third-order tensor $\hat{\mathcal{T}} = \llbracket \mathbf{G}, \mathbf{H}, \mathbf{P} \rrbracket$ that minimizes the weighted error with respect to the observed data \mathcal{T}_{obs} at the known entries. The optimization problem is formulated as:

$$\min_{\mathbf{G}, \mathbf{H}, \mathbf{P}} \|\mathcal{W}_{\mathcal{T}} \times (\llbracket \mathbf{G}, \mathbf{H}, \mathbf{P} \rrbracket - \mathcal{T}_{obs})\|_F^2, \quad (13)$$

This is a standard weighted PARAFAC decomposition problem for data with missing entries, which can be solved efficiently using ALS.

3.2. Algorithm Derivation via ALS

We alternately optimize one factor matrix while fixing the other two. Updating the factor matrix \mathbf{G} while keeping \mathbf{H} and \mathbf{P} fixed, the mode-1 unfolding (matricization) of $\hat{\mathcal{T}}$ is given by:

$$\hat{\mathbf{T}}_{(1)} = \mathbf{G} (\mathbf{P} \odot \mathbf{H})^\top, \quad (14)$$

where \odot denotes the Khatri–Rao product. The cost function then becomes:

$$\min_{\mathbf{G}} \|\mathbf{W}_{\mathcal{T},(1)} \odot (\mathbf{T}_{obs,(1)} - \mathbf{G}(\mathbf{P} \odot \mathbf{H})^\top)\|_F^2, \quad (15)$$

This problem can be solved independently for each row \mathbf{g}_i^T of \mathbf{G} . For the i -th row:

$$\min_{\mathbf{g}_i^T} \sum_{j,k \text{ s.t. } w_{ijk}=1} |t_{obs,ijk} - \mathbf{g}_i^T (\mathbf{p}_j \odot \mathbf{h}_k)|^2, \quad (16)$$

where $\mathbf{p}_j^T, \mathbf{h}_k^T$ are row vectors of \mathbf{P} and \mathbf{H} , respectively. This is a standard weighted least-squares problem with solution given by the normal equations:

$$\begin{aligned} \mathbf{g}_i^T & \left(\sum_{(j,k) \in \Phi_i} (\mathbf{p}_j \odot \mathbf{h}_k)(\mathbf{p}_j \odot \mathbf{h}_k)^H \right) \\ & = \sum_{(j,k) \in \Phi_i} t_{obs,ijk} (\mathbf{p}_j \odot \mathbf{h}_k)^H, \end{aligned} \quad (17)$$

where Φ_i is the set of index pairs (j, k) satisfying $w_{ijk} = 1$. Letting $\mathbf{Z} = \mathbf{P} \odot \mathbf{H}$, the above can be written more compactly:

$$\mathbf{g}_i^T \leftarrow (\mathbf{T}_{obs,i,:} \mathbf{W}_{\mathcal{T},i} \mathbf{Z}^*) (\mathbf{Z}^T \mathbf{W}_{\mathcal{T},i} \mathbf{Z}^*)^{-1}, \quad (18)$$

where $\mathbf{W}_{\mathcal{T},i}$ is a diagonal matrix with diagonal elements from the i -th slice of the mask.

The updates for \mathbf{H} and \mathbf{P} follow symmetrically. For example, when updating \mathbf{H} , we fix \mathbf{G} and \mathbf{P} and solve the weighted least-squares problem with respect to \mathbf{H} .

3.3. DOA Estimation from Tensor Completion Results

Algorithm 1 TCDA Based on ALS

- 1: **Input:** Incomplete third-order tensor \mathcal{T}_{obs} , mask tensor $\mathcal{W}_{\mathcal{T}}$, desired rank R .
 - 2: **Initialize:** Randomly initialize factor matrices $\mathbf{G}^{(0)}, \mathbf{H}^{(0)}, \mathbf{P}^{(0)}$.
 - 3: **repeat**
 - 4: **Update G:** Fix $\mathbf{H}^{(t)}, \mathbf{P}^{(t)}$, solve for each row update according to (6) to obtain $\mathbf{G}^{(t+1)}$.
 - 5: **Update H:** Fix $\mathbf{G}^{(t+1)}, \mathbf{P}^{(t)}$, symmetrically solve to update $\mathbf{H}^{(t+1)}$.
 - 6: **Update P:** Fix $\mathbf{G}^{(t+1)}, \mathbf{H}^{(t+1)}$, symmetrically solve to update $\mathbf{P}^{(t+1)}$.
 - 7: **until** The fitted DOA error is less than the threshold of 1° .
 - 8: **Output:** Estimated factor matrices $\hat{\mathbf{G}}, \hat{\mathbf{H}}, \hat{\mathbf{P}}$.
-

The direct output of Algorithm 1 is the estimated factor matrices $\{\hat{\mathbf{G}}, \hat{\mathbf{H}}, \hat{\mathbf{P}}\}$. No additional PARAFAC decomposition is required. The DOA information is directly contained in factor matrix $\hat{\mathbf{H}} \in \mathbb{C}^{4 \times R}$.

We can directly extract angular information from the elements of the k -th column $\hat{\mathbf{h}}_k$ of $\hat{\mathbf{H}}$. The azimuth-related term $\Theta_k = e^{j\pi \cos \theta_k}$ can be estimated as $\hat{\Theta}_k = \hat{h}_{k,2}/\hat{h}_{k,1}$, while the elevation-related term $\Phi_k = e^{j\pi \cos \phi_k}$ is obtained through $\hat{\Phi}_k = (\hat{h}_{k,3}/\hat{h}_{k,1})^{-1}$. Subsequently, the actual DOA angles are recovered from these phase terms through:

$$\hat{\theta}_k = \arccos \left(\frac{\text{angle}(\hat{\Theta}_k)}{\pi} \right), \hat{\phi}_k = \arccos \left(\frac{\text{angle}(\hat{\Phi}_k)}{\pi} \right) \quad (19)$$

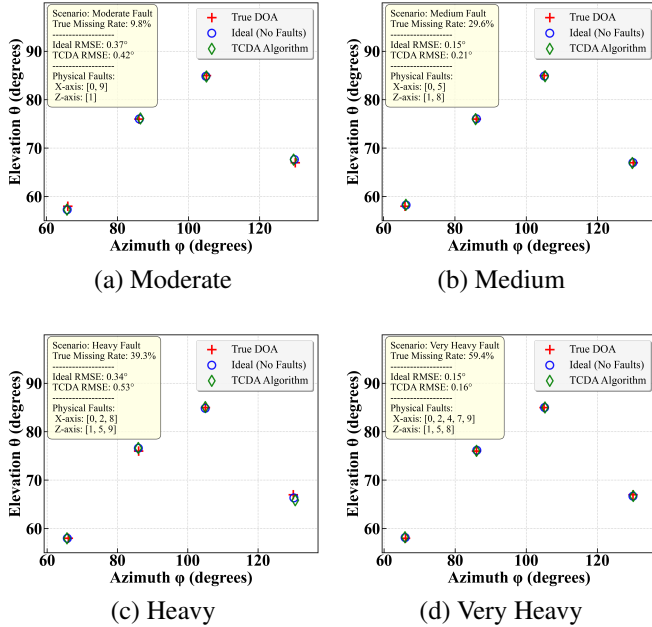


Fig. 1. DOA estimation scatter plots under four fault scenarios at SNR = 10 dB.

This extraction process is performed for each column of $\hat{\mathbf{H}}$ to obtain all automatically paired 2D DOA estimates $\{(\hat{\phi}_k, \hat{\theta}_k)\}_{k=1}^R$.

4. SIMULATION RESULTS

To comprehensively evaluate the performance of the proposed algorithm, a series of simulations were conducted. All experiments are based on an L-shaped array with $M = 10$ elements, receiving signals from $K = 4$ far-field narrowband sources. The true Directions-of-Arrival (DOAs) of the sources are set to $(58^\circ, 66^\circ)$, $(67^\circ, 130^\circ)$, $(76^\circ, 86^\circ)$, and $(85^\circ, 105^\circ)$. The number of snapshots is $N_{\text{snapshots}} = 500$. To ensure statistical reliability, all performance results were obtained by averaging over 1000 independent Monte Carlo trials.

Fig. 1 presents the DOA estimation scatter plots for a fixed SNR of 10 dB across four scenarios of increasing severity, visually demonstrating the algorithm’s resilience. Even with moderate physical damage resulting in 9.8% missing data in the target tensor (Fig. 1 (a)), the TCDA estimates (green diamonds) remain tightly clustered around the true DOAs, with an RMSE of 0.20° that is remarkably close to the ideal 0.14° bound. As the damage intensifies to a medium fault level, causing a significant 29.6% data loss (Fig. 1 (b)), the algorithm’s robustness persists, maintaining an excellent RMSE of 0.22° .

This resilience is further tested under a heavy fault scenario (Fig. 1 (c)), where nearly 40% of the tensor data is unavailable. While a slight increase in estimation variance is

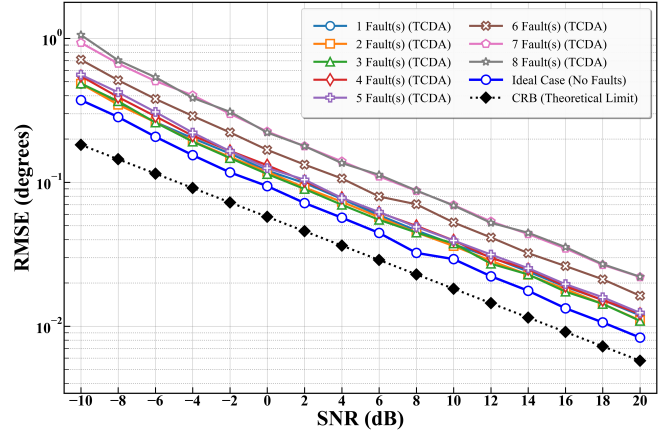


Fig. 2. RMSE performance versus SNR for different numbers of faulty sensors.

visible, TCDA’s RMSE of 0.33° confirms it still resolves all sources accurately. The framework’s true power is showcased in the extreme stress test of a very heavy fault (Fig. 1 (d)). Here, despite a staggering 59.4% of the data being missing—a condition under which traditional methods would catastrophically fail—our algorithm remains operational, providing usable estimates with an RMSE of 0.39° . Collectively, these results provide compelling evidence of the TCDA framework’s “self-healing” capability. The algorithm’s performance degrades gracefully as physical damage increases, effectively bridging the gap between catastrophic failure and the performance of a perfect array, making it a highly practical solution for real-world applications.

To further investigate the performance of the TCDA algorithm under varying noise levels and for different numbers of faults, we conducted a second set of experiments, with the results presented in Fig. 2. The figure plots the RMSE as a function of SNR, ranging from -10 dB to 20 dB, for scenarios with 1 to 8 randomly faulty sensors.

As is evident from the figure, all performance curves behave consistently: the RMSE decreases monotonically as the SNR increases, and all curves lie above the Cramér-Rao Bound (CRB). Contrary to typical sub-optimal estimators, the curves do not exhibit distinct “error floors” in the high-SNR region; instead, they maintain a parallel descent relative to the ideal case and the CRB. The performance limits are distinctly categorized by the severity of the lost spatial information. For mild to moderate damage (1 to 5 faulty sensors), the performance curves are tightly clustered and closely follow the curve for the ideal (no-faults) case across the entire SNR spectrum, indicating that the tensor completion effectively compensates for the missing data. In contrast, for severe fault scenarios (6 to 8 faults), the curves clearly separate from the ideal case, reflecting the fundamental performance limit imposed by substantial spatial information loss.

The most crucial insight from this figure is the "graceful degradation" property exhibited by the TCDA algorithm. Performance does not collapse catastrophically after a few faults; instead, it declines smoothly and predictably as the number of faults increases. Notably, with 1 to 5 faulty sensors, the algorithm suffers virtually no performance loss compared to the ideal case. Even in the extreme stress test of 8 faulty sensors, the algorithm maintains robust performance, keeping the RMSE well below 1° for any SNR above -8 dB (e.g., 0.70° at -8 dB). This predictable and smooth performance decline confirms that the algorithm is a highly reliable and robust choice for applications facing varying noise conditions and inevitable hardware failures.

5. CONCLUSION

This paper introduces the TCDA framework, an innovative solution for robust 2D-DOA estimation with defective sensor arrays. We transform the physical fault problem into a standard weighted PARAFAC decomposition task by modeling the incomplete third-order target tensor from the defective signals. This approach is both theoretically elegant and computationally efficient, as its output factor matrices are directly used for DOA extraction, eliminating extra parameter pairing steps. A detailed derivation of the ALS-based solver is provided. Extensive simulations confirm that TCDA effectively recovers the incomplete spatial data, exhibiting a remarkable "graceful degradation" property. Notably, the algorithm entirely avoids the error floors typical of sub-optimal estimators and maintains estimation accuracy approaching that of a flawless array even when half of the sensors are defective. This research opens new avenues for developing highly reliable, fault-tolerant sensor systems for complex operational environments.

6. REFERENCES

- [1] J. Li and P. Stoica, "MIMO radar with colocated antennas," *IEEE Signal Processing Magazine*, vol. 24, no. 5, pp. 106–114, September 2007.
- [2] A. Haimovich, R. S. Blum, and L. J. Cimini Jr., "MIMO radar with widely separated antennas," *IEEE Signal Processing Magazine*, vol. 25, no. 1, pp. 116–129, January 2008.
- [3] Y. Hua, T. K. Sarkar, and D. D. Weiner, "An L-shaped array for estimating 2-D directions of wave arrival," *IEEE Transactions on Antennas and Propagation*, vol. 39, no. 2, pp. 143–146, February 1991.
- [4] R. A. Harshman, "Foundations of the PARAFAC procedure: Model and conditions for an 'explanatory' multi-mode factor analysis," *UCLA Working Papers in Phonetics*, vol. 16, pp. 1–84, 1970.
- [5] P. Pal and P. P. Vaidyanathan, "Nested arrays: A novel approach to array processing with enhanced degrees of freedom," *IEEE Transactions on Signal Processing*, vol. 58, no. 8, pp. 4167–4181, August 2010.
- [6] T. G. Kolda and B. W. Bader, "Tensor decompositions and applications," *SIAM Review*, vol. 51, no. 3, pp. 455–500, 2009.
- [7] David L Donoho, "Compressed sensing," *IEEE Transactions on information theory*, vol. 52, no. 4, pp. 1289–1306, 2006.
- [8] R. T. Hoctor and S. A. Kassam, "The unifying role of the coarray in aperture synthesis for coherent and incoherent imaging," *Proceedings of the IEEE*, vol. 78, no. 4, pp. 735–752, April 1990.
- [9] Y. Y. Dong, C. x. Dong, W. Liu, H. Chen, and G. q. Zhao, "2-D DOA estimation for L-shaped array with array aperture and snapshots extension techniques," *IEEE Signal Processing Letters*, vol. 24, no. 4, pp. 495–499, April 2017.
- [10] T. Jiang, N. D. Sidiropoulos, and J. M. F. ten Berge, "Almost sure identifiability of multidimensional harmonic retrieval," *IEEE Transactions on Signal Processing*, vol. 49, no. 9, pp. 1849–1859, September 2001.
- [11] G. Tomasi and R. Bro, "A comparison of algorithms for fitting the PARAFAC model," *Computational Statistics & Data Analysis*, vol. 50, no. 7, pp. 1700–1734, 2006.
- [12] Wenlong Wang and Lei Zhang, "DOA estimation for coherent and non-coherent mixed signals using Toeplitz diagonal diffusion," *IEEE Signal Processing Letters*, vol. 32, pp. 1985–1989, 2025.
- [13] A. Cichocki, D. Mandic, L. De Lathauwer, G. Zhou, Q. Zhao, C. Caiafa, and H. A. Phan, "Tensor decompositions for signal processing applications," *IEEE Signal Processing Magazine*, vol. 32, no. 2, pp. 145–163, March 2015.
- [14] D. Nion and N. D. Sidiropoulos, "A PARAFAC-based technique for detection and localization of multiple targets in a MIMO radar system," in *Proc. IEEE Int. Conf. Acoust., Speech Signal Process. (ICASSP)*, pp. 2077–2080, April 2009.
- [15] Wei Rao, Dan Li, and Jian Qiu Zhang, "A Tensor-Based Approach to L-Shaped Arrays Processing With Enhanced Degrees of Freedom," *IEEE Signal Processing Letters*, vol. 25, no. 2, pp. 277–281, February 2018.